JVST A
Journal of Vacuum Science & Technology A

ARTICLE

avs.scitation.org/journal/jva

Effects of adventitious impurity adsorption on oxygen interstitial injection rates from submerged TiO_2(110) and ZnO(0001) surfaces

Cite as: J. Vac. Sci. Technol. A 41, 033203 (2023); doi: 10.1116/6.0002467
Submitted: 31 December 2022 · Accepted: 27 February 2023 ·
Published Online: 21 March 2023

Heonjae Jeong[1] and Edmund G. Seebauer[2,a)]

AFFILIATIONS

[1]Department of Mechanical Science and Engineering, University of Illinois at Urbana-Champaign, Urbana, Illinois 61801
[2]Department of Chemical and Biomolecular Engineering, University of Illinois at Urbana-Champaign, Urbana, Illinois 61801

[a)]**Author to whom correspondence should be addressed:** eseebaue@illinois.edu

ABSTRACT

Low bond coordination of surface atoms facilitates the injection of oxygen interstitial atoms into the bulk near room temperature from the clean surfaces of semiconducting metal oxides when exposed to liquid water, opening new prospects for postsynthesis defect engineering and isotopic fractionation. The injection rate and penetration depth vary considerably under identical experimental conditions, however, with the adsorption of adventitious carbon suggested as the cause. For water-submerged rutile TiO_2(110) and wurtzite ZnO(0001), this work bolsters and refines that hypothesis by combining the isotopic self-diffusion measurements of oxygen with characterization by x-ray photoelectron spectroscopy and atomic force microscopy. Adventitious carbon likely diminishes injection rates by poisoning small concentrations of exceptionally active surface sites that either inject O or dissociate adsorbed OH to injectable O. These effects propagate into the penetration depth via the progressive saturation of O_i traps near the surface, which occurs less extensively as the injected flux decreases.

I. INTRODUCTION

Exposure of specially prepared semiconducting oxide surfaces to liquid water promotes the injection of mobile oxygen interstitial atoms (O_i) that enable high levels of diffusive isotopic fractionation[1] as well as postsynthesis engineering of defects in oxides near room temperature.[2] Isotopic fractionation is useful for enhanced thermal conduction[3–7] and for quantum computing and sensing.[6–8] Defect engineering with O_i helps to compensate extrinsic donors[8] such as H.[2] In addition, O_i annihilates oxygen vacancies (V_O) that influence electrical conductivity,[9,10] ferromagnetism,[11] superconductivity,[12] chemical reactivity,[13,14] and charge carrier lifetimes[13,14] for applications in photocatalysis,[13–15] photoelectrochemistry,[10,13–15] advanced electronics,[11,13,16–18] and renewable energy production and storage.[13–15,19] The isotopic fractionation or defect engineering occurs near room temperature, thereby enabling both straightforward processing and access to an unexplored regime wherein kinetic effects far from equilibrium dominate the behavior.

Recent work points to many factors that influence the O_i injection rate and penetration depth.[1] For example, adventitious impurity adsorption poisons injection sites[20,21] and affects acid–base reactions between the surface and water that lead to surface charge buildup.[1] The charge buildup propagates into drift forces on charged interstitials[22] and into the stability of charged complexes that O_i forms with hydrogen[2] and other native or extrinsic defects.[23] Differences in injection behavior among crystallographic orientations[2,20] suggest a role for surface morphology, surface reconstructions, or roughness. Modeling of these effects will probably require process simulators akin to those developed for ion-implantation in microelectronic devices.[17,18]

Of immediate concern, however, is the random variability that manifests in isotopic self-diffusion measurements that are the workhorse technique for investigating these effects. A detailed statistical study for rutile TiO_2 has recently shown that nominally identical surface preparation procedures and diffusion conditions routinely yield net injection fluxes (F) with a standard deviation equivalent to a factor of 1.6.[24] For the mean diffusion length (λ), the corresponding factor is about 1.4.[24] ZnO and Ga_2O_3[2] exhibit roughly similar variations. However, reproducibility across a given specimen of TiO_2 exhibits a standard deviation only 25%–50% of

TABLE I. Solution compositions and preparation conditions for wet etching of TiO_2(110).

Solution	Composition (wt. %)	Time (min)	Temperature (°C)
Degreased-only	Acetone → isopropyl Alcohol → ethanol → methanol	—	25
Hydrogen peroxide	5% H_2O_2	5, 10, 20	25
	10% H_2O_2	5, 10, 20	25
NH_4OH	10% NH_4OH(aq)	40	25
Basic piranha	3:1 of 30% NH_4OH:30% H_2O_2	40	60
Sequential ammonia-peroxide	30% NH_4OH → 30% H_2O_2 → H_2O rinse	2 min each step	25
Phosphoric acid	85% H_3PO_4	10, 20, 40	80

that among different specimens. Since the adventitious adsorption of carbon around a single specimen probably varies less than among different specimens, this adsorption was proposed as the main contributor to experimental variability.[24]

This work bolsters and refines that hypothesis for rutile TiO_2(110) and wurtzite ZnO(0001). Isotopic self-diffusion measurements of oxygen during exposure to water are performed after surface preparation by various methods. Surfaces exhibiting large changes are characterized by x-ray photoelectron spectroscopy (XPS) and atomic force microscopy (AFM). The absence of impurities other than C, together with the lack of correlation between diffusion metrics and surface roughness or chemical state, suggests that adventitious C probably acts on injection rates by poisoning small concentrations of surface sites that are especially active for dissociating adsorbed OH to injectable O or for injecting O itself. These effects propagate into the penetration depth via the progressive saturation of O_i traps near the surface, which occurs less extensively as the injected flux decreases.

II. EXPERIMENT

Experiments employed single crystals of either rutile TiO_2(110) (MTI Corp.) or wurtzite Zn-terminated ZnO(0001) (CrysTec GmbH). AFM showed that the surfaces of both oxides before any surface preparation exhibited a roughness of <0.5 nm as specified by the manufacturer. Specimens were cut to dimensions of $5–10 \times 5 \times 0.5\ mm^3$. Surfaces were then prepared by various methods in an attempt to vary the injection rate outside the normal range of random variability and to vary the surface roughness.

A. Surface preparation

At the outset, all specimens were degreased by successive 10 min ultrasonic baths in reagent-grade acetone, isopropyl alcohol, ethanol, and methanol. In certain benchmark cases, only degreasing was performed with no other chemical treatment. "Degreased-only" denotes such specimens in the text below.

Several distinct protocols were employed for specimens that underwent wet etching. Table I summarizes the etchants used for TiO_2(110), and Table II summarizes the corresponding etchants for ZnO(0001). Broadly speaking, the etchants involved H_2O_2, NH_4OH, or combinations of the two at various concentrations, temperatures, and/or times. Final rinsing with de-ionized water was performed only in the case of a sequential etch employing $NH_4OH \rightarrow H_2O_2 \rightarrow H_2O$. For TiO_2, etchants based on phosphoric acid (H_3PO_4)[25] were also examined, but these were determined by subsequent XPS to deposit significant quantities of phosphorous. Adsorbed sulfur is known to impede oxygen self-diffusion in TiO_2 (Ref. 20) and ZnO,[21] and similar inhibition seems likely for phosphorous. Specimens exposed to these P-containing etchants did not undergo further investigation.

Specimens that underwent high-temperature vacuum annealing in O_2 were mounted in a stainless-steel ultrahigh vacuum chamber as described previously.[20,26] A Si/SiO_2 plate provided mechanical support and resistive heating. Temperature was monitored with a chromel–alumel thermocouple press fitted directly to the specimen's front surface. After degreasing, vacuum annealing took place under O_2 gas (99.995%) of natural isotopic abundance for 4h; TiO_2(110) was annealed at $T = 450$ °C and $P_{O_2} = 5.0 \times 10^{-6}$ Torr, and ZnO(0001) was annealed at $T = 500$ °C and $P_{O_2} = 1.0 \times 10^{-5}$ Torr.

B. Isotopic self-diffusion

Specimens were immersed in ^{18}O-labeled water H_2O (10 at. % ^{18}O, Sigma-Aldrich) at temperatures ranging from 30 to 80 °C for 1h in an atmospheric environment. Typically, 1–2h elapsed between the end of an etching or annealing protocol and the start of a diffusion experiment. The ^{18}O concentration profiles were measured *ex situ* by time-of-flight secondary ion mass spectrometry (TOF-SIMS) with a PHI-TRIFT III instrument employing a Cs ion beam source operating at 3 keV.

TABLE II. Solution compositions and preparation conditions for wet etching of ZnO (0001).

Solution	Composition (wt. %)	Time (min)	Temperature (°C)
Degreased-only	Acetone → isopropyl Alcohol → ethanol → methanol	—	25
Hydrogen peroxide	10% H_2O_2	5, 10, 20	25, 80
	20% H_2O_2	5, 10, 20	25, 80
	30% H_2O_2	5, 10, 20	25, 80
NH_4OH	10% NH_4OH(aq)	40	25

Several metrics were computed from the profiles. Slopes of the deep-bulk profiles plotted on a semilogarithmic scale yielded λ as described elsewhere.[20,26,27] Because several kinds of trapping sites may be present, λ represents a phenomenological parameter as discussed elsewhere.[1] F was calculated by the integration of the entire area encompassed between the measured ^{18}O concentration and the natural abundance of ^{18}O (0.2%). Since 10% isotopically pure water was used, the computation of F included a factor of 10 to represent the total injected flux of both isotopes. The penetration depth (L) of ^{18}O was determined as the depth near the outmost limit of the profile at which the ^{18}O concentration reached 1.30×10^{20} cm^{-3}. This concentration slightly exceeds the natural abundance baseline concentration of ^{18}O (1.27×10^{20} cm^{-3}) and enables a precise (albeit arbitrary) definition of the "end" of a profile whose shape declines asymptotically to the baseline.

C. Surface characterization

The surface morphology and roughness were measured before isotopic self-diffusion by AFM with an MFP-3D instrument in tapping mode. In all cases, specimens were removed from the liquid and dried in a flowing N_2 gas to remove any remaining droplets that adhered. For accurate comparison between specimens, the Al-coated silicon probes (Ted Pella Inc.) were changed for every measurement. Each measurement generated 512×512 data points.

Surface chemical composition was measured after isotopic diffusion by XPS with a Kratos Axis ULTRA instrument. The XPS measurements employed a monochromatic Al Kα source (1486.6 eV). Spectral energies were calibrated based on the C_{1s} peak of adventitious carbon at 284.6 eV. Elemental compositions were quantified from peak areas together with sensitivity factors provided by the CasaXPS software library.

Peaks corresponding to individual elements typically comprised several incompletely resolved components whose energies vary with chemical state. These component peaks were deconvolved by Gaussian curve fitting employing software provided by the instrument manufacturer. SIMS measurements leave adsorbed Cs on the surface, so XPS was performed before the SIMS measurements. In some cases involving difficulties in instrument scheduling, XPS was done on specimens differing from those measured with SIMS. In such cases, XPS was done on specimens exposed to preparation and diffusion conditions matching those for which SIMS profiles were measured.

III. RESULTS

A. Effects of surface treatment on diffusion behavior

1. TiO_2

Before examining the effects of preparation procedure, we checked to what extent SIMS profiles before submersion matched an ideal in which ^{16}O and ion fragments containing Ti are spatially uniform everywhere and identical among different locations. No C- or H-containing fragments should appear. Figure 1 shows actual ion current profiles for an array of ^{16}O- and C-containing ion fragments from several representative locations on a single TiO_2(110) specimen that underwent only degreasing. The ^{16}O and TiO profiles vary with depth and among locations but only in the first

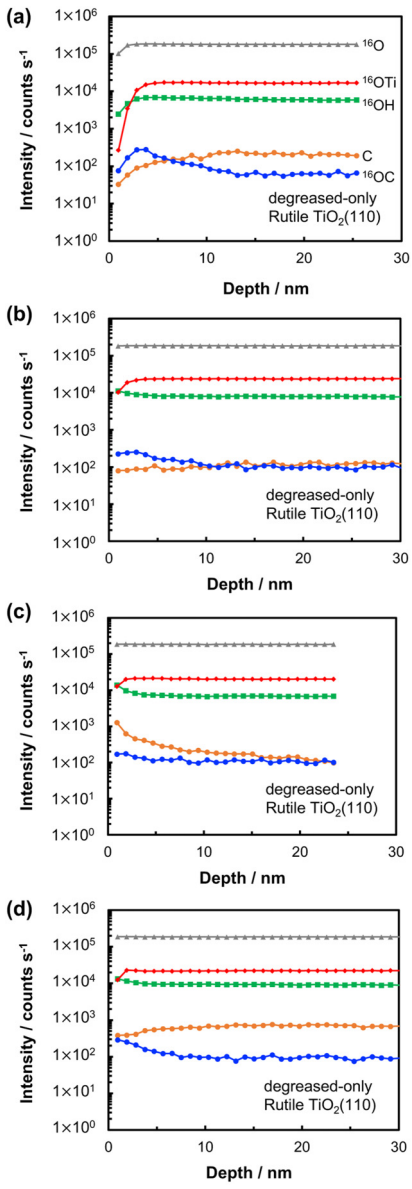

FIG. 1. (a)–(d) Representative SIMS ion current profiles of ^{16}O, ^{16}O diatomic fragments ($^{16}O^{48}Ti$, ^{16}OH, ^{16}OC), and C at various locations on a single specimen of TiO_2(110) subjected only to degreasing (no water immersion). ^{48}Ti is the most abundant isotope of Ti and, therefore, yields the largest ion currents. The labels identifying various species are shown in (a). The ^{16}O and ^{16}OTi profiles vary with depth and among locations, but only in the first 1–3 nm. OH varies in the first 2–5 nm and among locations. The fragments C and ^{16}OC exhibit much more variation among locations that extends down to 10–15 nm. In principle, depth resolution in SIMS lies somewhat below 1 nm with the use of low incident ion energies <150 eV[28] and extremely smooth surfaces. As shown in the main text, the root mean square (RMS) roughness for all TiO_2 surfaces remained below 0.25 nm. However, the Cs ion beam operating at 3 keV probably caused collisional intermixing effects[28] that varied among measurements due to residual thin layers of extrinsic carbon species. Such effects presumably persist in SIMS measurements performed after self-diffusion.

1–3 nm. The profiles for ^{16}OH vary in the first 2–5 nm and among locations. The fragments C and ^{16}OC exhibit much more variation that extends down to 10–15 nm.

Figure 2(a) shows the example ^{18}O concentration profiles for TiO_2(110) after submersion and diffusion at 70 °C. The profiles vary in shape and spatial extent depending upon the initial treatment procedure. The primary metrics examined in this work depend on either the entire profile (F) or the deep-bulk portion of it (λ, L). The near-surface region within the first 5–7 nm often exhibits depletion in ^{18}O due to isotopic fractionation.[1] Differences among profiles also occur in this region, although the shapes respond to a sizable number of physical and chemical factors[1] that are complicated by challenges to SIMS metrology that become more pronounced near the surface.[29,30] Collisional mixing[28] due to the 3 keV Cs beam represents a primary example. This work focuses mainly on profile metrics that are less affected by such factors.

Figures 2(b)–2(d) show F, λ, and L for TiO_2 at fixed diffusion conditions in response to varying preparation procedures. At least three profiles were collected at different locations on a given specimen and in some cases on multiple specimens. The bars represent the value of each parameter averaged over all profiles. The confidence intervals represent standard errors derived from experiments with several dozen specimens described elsewhere, wherein wet etching with NH_4OH was used.[1,24] These confidence intervals embody a good representation of the variability that can be expected among large numbers of TiO_2 specimens. SIMS profiles taken at various points on a single specimen's surface exhibit confidence intervals that are much narrower regardless of preparation procedure—typically 25%–50% of those shown in Fig. 2.

Some of the preparation procedures shown in Fig. 2 yield parameters lying outside the standard errors of one another. For F, for example, pretreatment with NH_4OH and vacuum annealing give noticeably larger values than H_2O_2 treatment. NH_4OH also exceeds degreased-only. For λ, NH_4OH and perhaps vacuum annealing give larger values than 5% H_2O_2 and degreased-only. For L, NH_4OH and vacuum annealing give larger values than H_2O_2 and degreased-only. NH_4OH also exceeds basic piranha.

Figure 2 suggests NH_4OH and vacuum annealing yield roughly similar results for F, λ, and L in TiO_2. However, the two procedures give different initial concentrations of point defects in the bulk, particularly of oxygen vacancies (V_O). V_O are largely eliminated during vacuum annealing with small amounts of O_2 present, whereas this elimination does not occur for wet etching with NH_4OH, demonstrating that initial conditions affect near-surface isotopic fractionation.[24] We, therefore, undertook a set of experiments to measure F, λ, and L for TiO_2 over a wider range of diffusion temperatures to (1) determine whether the temperature dependence differs for NH_4OH vs annealing and (2) seek statistically significant changes that would be undetectable by the simple inspection of confidence intervals. Figure 3 shows the data obtained for each parameter in Arrhenius form. The corresponding activation energies appear in Table III. The means lie within each other's standard error.

However, the visual inspection of Fig. 3(b) suggests that the mean values for λ averaged over all temperatures, and especially at

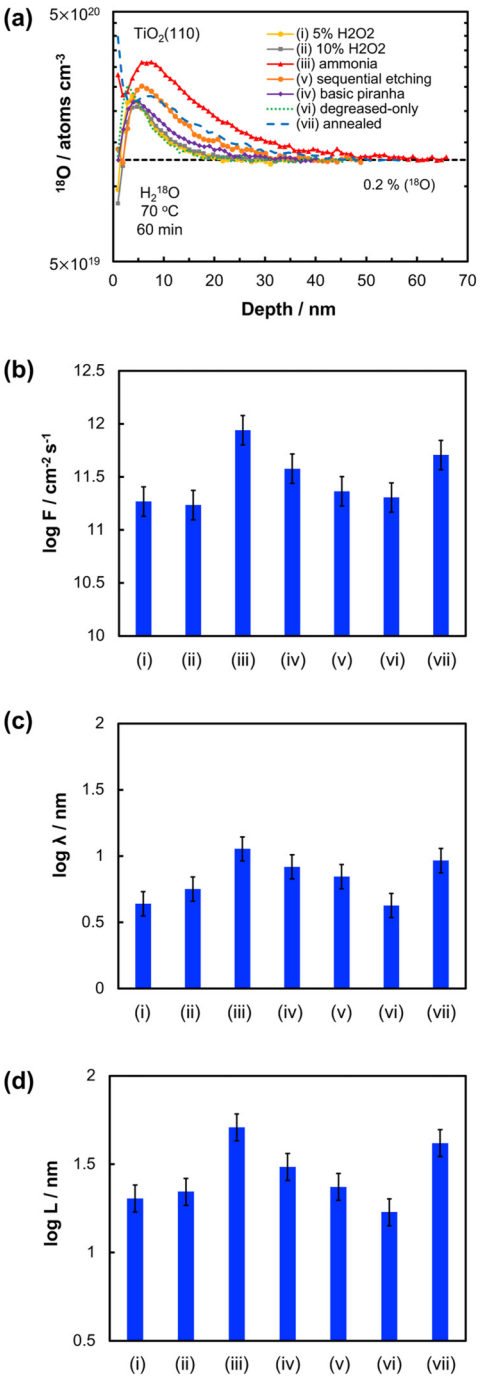

FIG. 2. (a) ^{18}O concentration profiles for TiO_2(110) treated by various methods. Diffusion time was 1h at 70 °C. Kinetic parameters in (b)–(d) include the net injection flux (F), mean diffusion length (λ), and the penetration depth (L). In (b)–(d), the x axis labels represent the surface preparation using (i) 5% H_2O_2 at 25 °C for 20 min, (ii) 10% H_2O_2 at 25 °C for 20 min, (iii) NH_4OH solution at 25 °C for 40 min, (iv) sequence of NH_4OH and 30% H_2O_2, (v) basic piranha, (vi) degreased-only, and (vii) vacuum annealed.

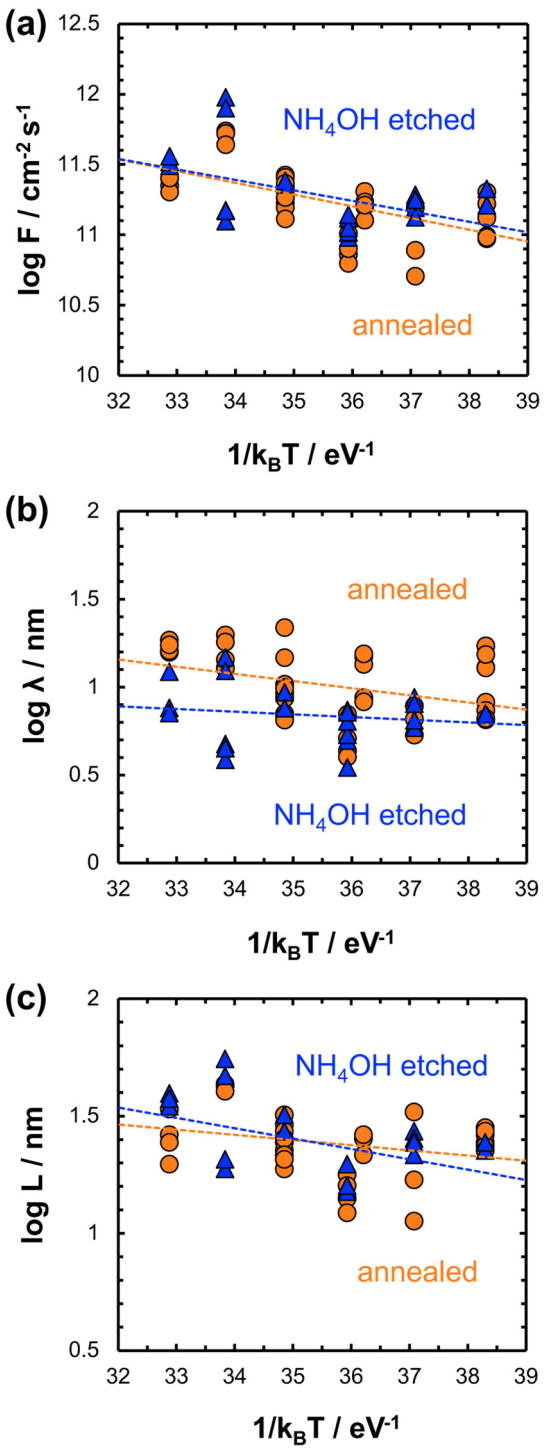

FIG. 3. Comparison of parameters for NH_4OH-etched and vacuum-annealed surfaces of TiO_2(110), including (a) net injection flux F, (b) mean diffusion length λ, and (c) penetration depth L. Triangles denote NH_4OH etching, and circles signify vacuum annealing.

TABLE III. Activation energy of kinetic parameters for NH_4OH-etched and vacuum annealed TiO_2(110).

	Activation energy (eV)	
Parameters	NH_4OH-etched	Annealed
F (cm^{-2} s^{-1})	0.17 ± 0.07	0.19 ± 0.04
λ(nm)	0.03 ± 0.04	0.09 ± 0.03
L (nm)	0.10 ± 0.04	0.05 ± 0.02

high temperature, for annealed specimens are higher than those for NH_4OH-treated specimens. A conceptually straightforward way to make this comparison with statistical rigor employs the regression lines to estimate the value of each data point scaled to the mean temperature (about 58 °C for the entire data set). This scaling procedure quantitatively preserves the standard error characterizing the scatter around the regression lines and enables the use of Student's t-test to compare the means of the two procedures. The comparison of conventional t-statistics for the two data sets for λ yielded a two-tailed p-value of 0.0012 for the entire temperature range and 0.086 for diffusion temperatures of 60 °C and above. In other words, the likelihood that the difference in means resulted from pure chance is 0.12% for the entire data set and 0.86% for high temperatures. These values offer compelling evidence that vacuum annealing yields slightly higher values of λ than NH_4OH pretreatment. No statistically significant difference could be found from comparable t-tests for F and L.

2. ZnO

Figure 4(a) shows the example ^{18}O concentration profiles for ZnO diffusion at 70 °C. As with TiO_2, the profiles vary in shape and spatial extent depending upon the initial treatment procedure. Figures 4(b)–4(d) show F, λ, and L for ZnO at fixed diffusion conditions in response to varying preparation procedures. As for TiO_2, at least three profiles were collected at different locations on a given specimen and in some cases on multiple specimens. The bars represent the value of each parameter averaged over all profiles. The confidence intervals represent standard errors derived from the wet etching experiments where the surface was prepared with 10% H_2O_2 for 20 min at 80 °C using numerous samples described elsewhere[2] and resemble the results seen with TiO_2. As with TiO_2, SIMS profiles taken at various points on a single ZnO specimen's surface exhibit confidence intervals that are much narrower regardless of preparation procedure—typically 25%–50% of those shown in Fig. 4.

Some of the preparation procedures shown in Fig. 4 yield parameters lying outside the standard errors of one another. For F, for example, pretreatment with 10% H_2O_2 and vacuum annealing give noticeably larger values than 20% H_2O_2 and degreased-only. For λ and L, 10% H_2O_2 gives larger values than 20% H_2O_2 and NH_4OH, and 30% H_2O_2, and vacuum annealing also exceeds 20% H_2O_2 and degreased-only.

Some wet etching solutions were examined under varying conditions of time or etching temperature as shown in Table S1 in the supplementary material.[63] Figure S1 in the supplementary material[63] shows the results for three different concentrations

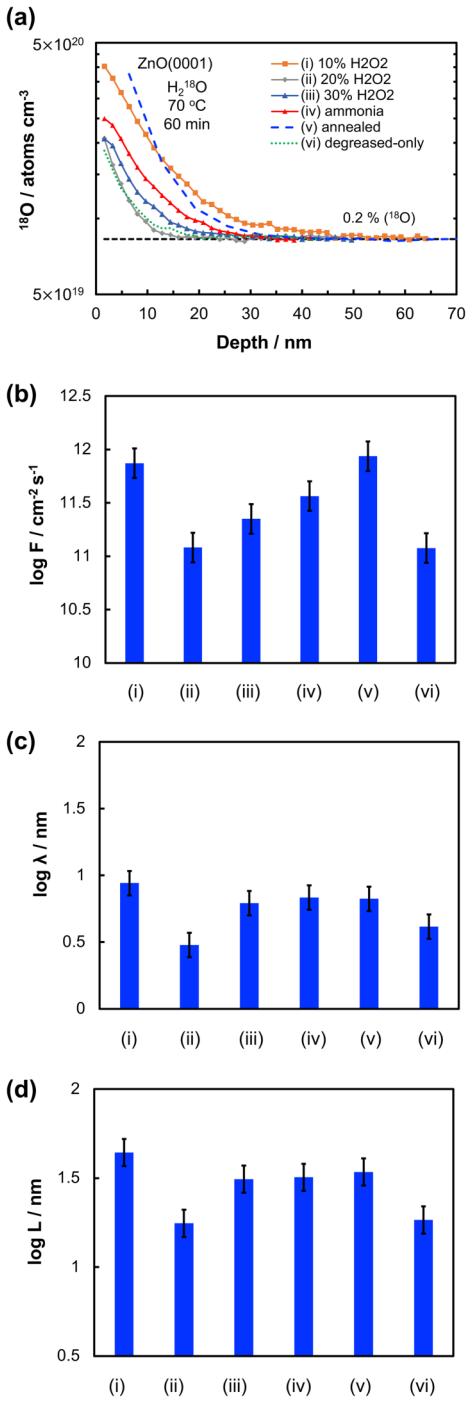

FIG. 4. (a) ^{18}O concentration profiles for ZnO(0001) treated by various methods. Diffusion time was 1h at 70 °C. Kinetic parameters in (b)–(d) include F, λ, and L. In (b)–(d), the x axis labels represent the surface preparation using (i) 10% H_2O_2 at 80 °C for 20 min, (ii) 20% H_2O_2 at 80 °C for 20 min, (iii) 30% H_2O_2 at 80 °C for 20 min, (iv) NH_4OH, (v) vacuum annealed, and (vi) degreased-only.

(10%, 20%, and 30% H_2O_2) at 25 °C and 20 min. At this lower temperature (compared to 80 °C in Fig. 4), the H_2O_2 concentration exerts no statistically significant effects on F, λ, or L. Figure S2 in the supplementary material[63] shows the results for 30% H_2O_2 at 25 °C for three different etching times (5, 10, and 20 min). Curiously, 10 min yields noticeably higher values of F, λ, and L than either 5 or 20 min.

B. Surface morphology

For TiO_2(110), AFM shows that surfaces become slightly smoother upon either vacuum annealing or NH_4OH etching (Fig. 5). The root mean square (RMS) roughness is 0.23 ± 0.03, 0.10 ± 0.02, and 0.14 ± 0.08 nm, respectively, for the degreased-only, vacuum annealed, and NH_4OH-etched material.

In contrast, vacuum annealing and H_2O_2 etching roughen ZnO(0001) relative to the degreased-only material (Fig. 6). The degreased-only RMS roughness is 0.21 ± 0.08 nm. However, vacuum annealing leads to 0.39 ± 0.01 nm and wet etching to 1.71 ± 0.1 nm. This last number matches the previous literature that reports 1–2 nm roughness for etching with 10% H_2O_2, and the roughness does not change significantly as the peroxide concentration increases.[31] Figure 6 shows that the lateral length scale of the roughness increases dramatically upon etching with H_2O_2, from about 20 to about 200 nm.

C. Surface composition

For TiO_2, survey XPS spectra were examined for three preparation procedures: as-degreased-only, vacuum annealed, and wet etched with NH_4OH. The spectra showed no evidence for the significant concentrations of elements other than Ti, O, and C. Narrow scan spectra of these three elements were obtained to determine the surface concentration and chemical state. Figure 7 shows that the concentration of O is two to three times higher than that of Zn, whereas the expected Ti:O ratio for a bulk-terminated surface is nominally 1:2. Any excess O probably resides in the adventitious adsorption of OH and oxygenates of carbon. In any case, the elemental surface concentrations did not change appreciably in response to the preparation procedure.

Deconvolution results for the individual chemical states are detailed in the supplementary material.[63] For Ti, the Ti_{2p} peaks point to the pure Ti^{4+} oxidation state (Fig. S3 in the supplementary material[63]). For O, the O_{1s} peaks comprise two components: Ti—O bonding and H—O, C—O, or a combination of the two (see Fig. S4 in the supplementary material[63]). For C, the C_{1s} peaks comprise three contributions: C—C (or C═C), C—O, and O—C═O (see Fig. S5 in the supplementary material[63]). The relative proportions of the chemical states (Fig. 8) showed no appreciable changes for any element in response to the preparation procedure.

We examined the XPS spectra of ZnO in an analogous way for degreased-only, vacuum annealing, and 10% H_2O_2 etching at 80 °C. The spectra showed no evidence for the significant concentrations of elements other than Zn, O, and C. Narrow scan spectra were obtained to determine the surface concentration and the chemical state. For Zn, we employed the Zn_{LMM} Auger peak because it exhibits better sensitivity than the Zn2p (~1021.2 eV).[32] Figure 7 shows that the concentration of O is two to three times

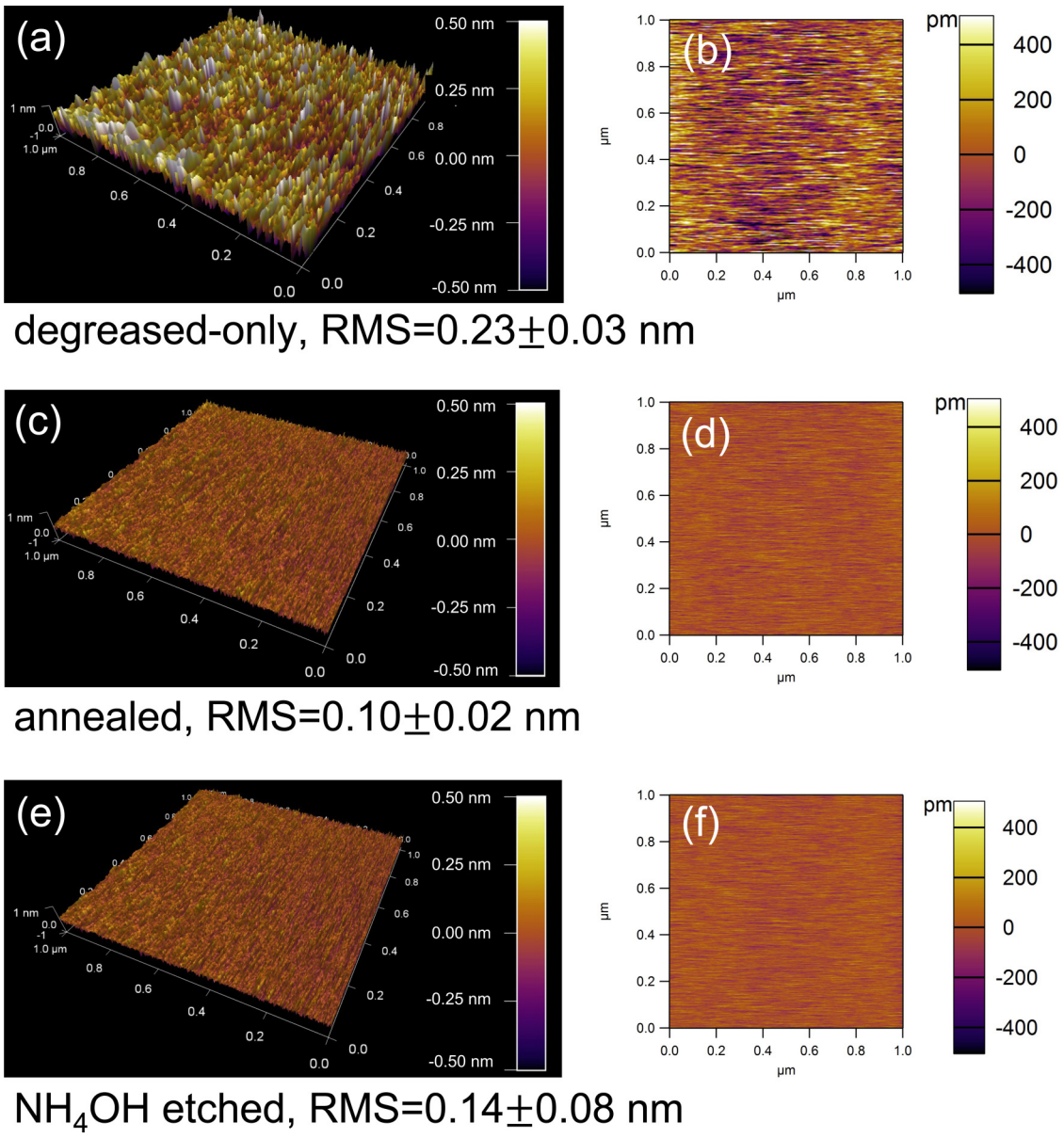

FIG. 5. Surface RMS roughness of TiO_2(110) prepared by various methods, shown in three- and two-dimensional forms for (a) and (b) degreased-only material, (c) and (d) vacuum annealing, and (e) and (f) NH_4OH wet etching.

higher than that of Zn, whereas the expected Zn:O ratio for a bulk-terminated Zn-rich surface is nominally a bit less than 1:1. The excess O probably resides in the adventitious adsorption of OH and oxygenates of carbon, to which Zn-ZnO(0001) is especially prone.[33] The concentration of Zn was perhaps a bit higher for samples that were degreased-only compared to those that were vacuum annealed, and the concentration of C was a bit lower, but the modest number of spectra contributing to the confidence intervals makes us reluctant to draw firm conclusions.

Deconvolution results for the individual chemical states are detailed in the supplementary material.[63] For Zn, the Zn_{LMM} Auger peak comprises two components (see Fig. S6 in the supplementary material[63]) that the literature has often ascribed to Zn—O bonding in the lattice and an interstitial-related species.[32,34,35] As for O in TiO_2, the O_{1s} peaks comprise two components: Zn—O bonding and H—O, C—O, or a combination of the two (Fig. S7 in the supplementary material[63]). For C, the C_{1s} peaks comprise three contributions from C—C (or C═C), C—O, and O—C═O (see Fig. S8 in

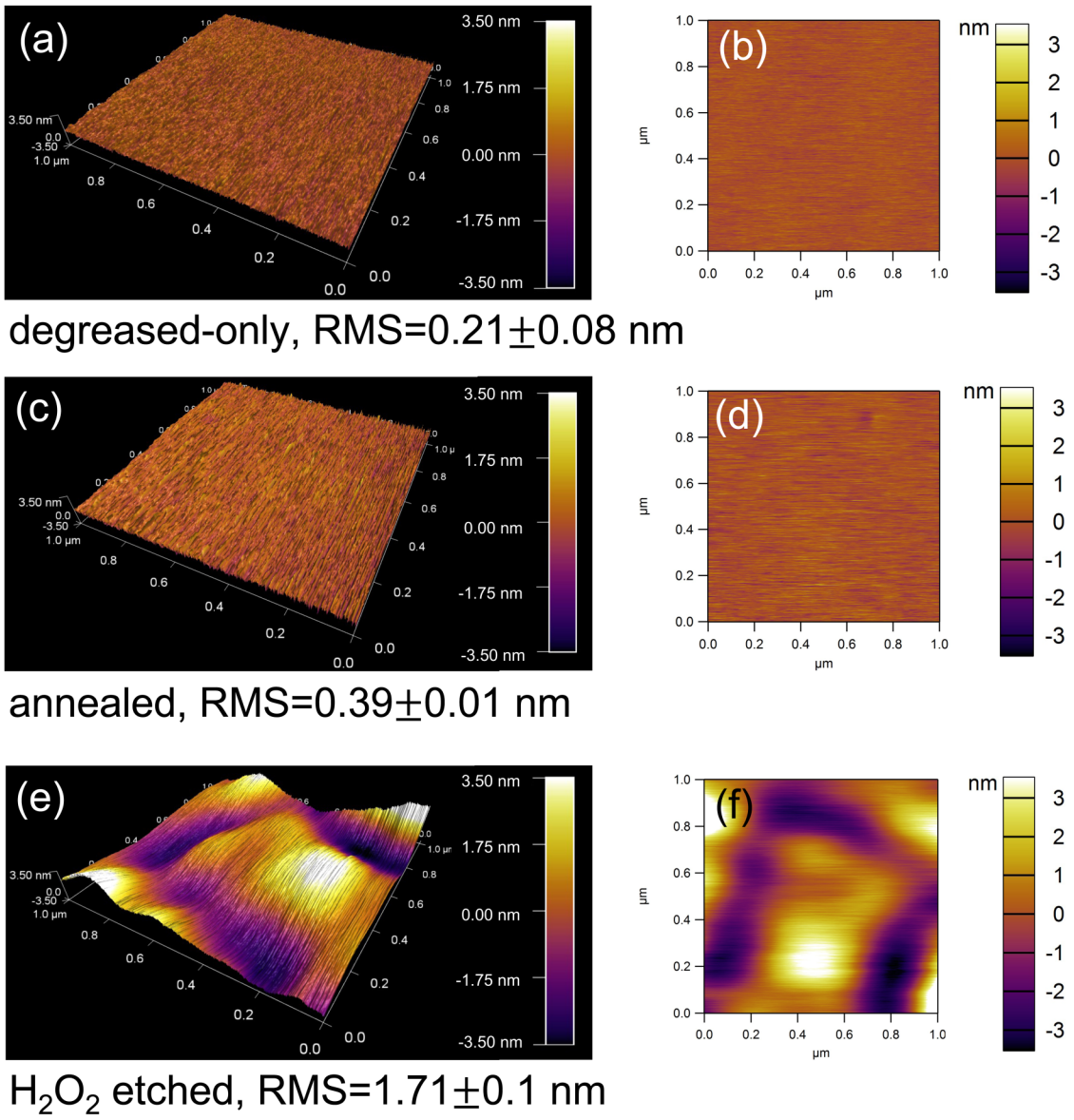

FIG. 6. Surface roughness of ZnO(0001) prepared by various methods, shown in three- and two-dimensional forms for (a) and (b) degreased-only material, (c) and (d) vacuum annealing, and (e) and (f) 10% H_2O_2 etching at 80 °C.

the supplementary material[63]). The relative proportions of the chemical states (Fig. 9) showed no convincing evidence of consistent change for any element in response to the preparation procedure.

IV. DISCUSSION

Existing literature for O_i injection shows a standard deviation in the profile metrics F and λ by a factor of about 1.5, remaining fairly consistent across the various oxides and crystallographic orientations examined so far.[2] This magnitude of variation far exceeds what can be attributed to instrumental effects in SIMS metrology. Differences in same-specimen vs different-specimen standard deviations hinted that difficult-to-control adventitious adsorption accounts for the variation.

Prior literature has reported considerable detail about the mechanism of O_i injection from both TiO_2(110) and ZnO(0001). For TiO_2, the relevant reconstruction is 1×1 under vacuum environments containing O_2 at the temperature of interest. The O_2 adsorbs and dissociates at special sites on the surface

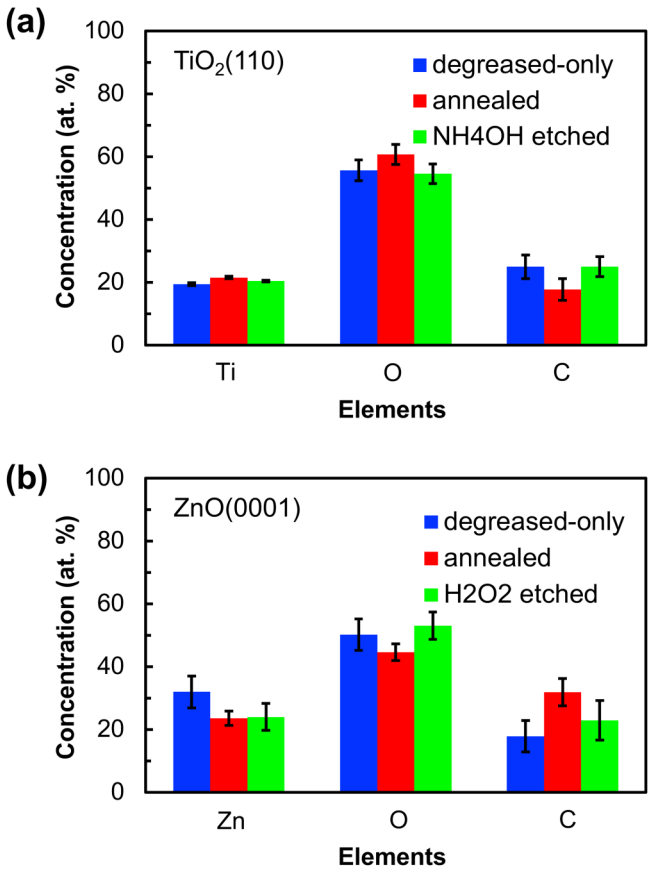

FIG. 7. Surface elemental composition shown as percentages from XPS measurements for (a) TiO_2(110) and (b) ZnO(0001) in response to various surface treatments, including degreased-only (blue), vacuum annealed (red), and wet etched (green). Wet etchant was NH_4OH for TiO_2 and 10% H_2O_2 at 80 °C for 20 min for ZnO. Confidence intervals were derived from data taken at various points on several specimens.

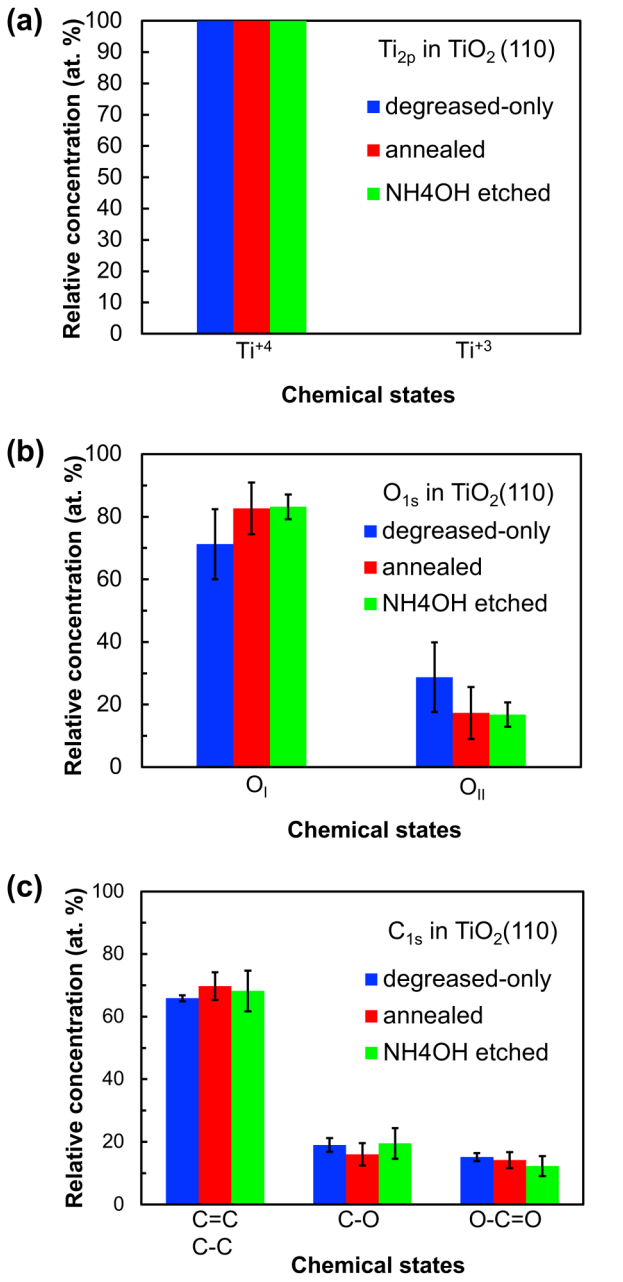

FIG. 8. Relative concentrations of different chemical states as measured by XPS on TiO_2(110) for (a) Ti, (b) O, and (c) C in response to various surface treatments. From left to right, bars signify degreased-only (blue), vacuum annealed (red), and wet etched (green). Confidence intervals were derived from data taken at various points on several specimens.

(perhaps steps or kinks), with atomic oxygen diffusing out onto terraces into either twofold or threefold bonding configurations that both lead to injection.[36,37] Aqueous environments are thought to preserve the 1×1 structure,[38] and water adsorbs as a combination of molecular H_2O and/or its dissociation products OH and H,[2,39–42] with only a small energy difference between the molecular and dissociated forms. Oxygen injects as atomic O, not as OH; deuterium labeling studies indicate that no hydrogen enters the material.[2]

For ZnO(0001), reconstruction in a vacuum environment containing O_2 yields a complicated n7n3 "triangular pit" structure.[43,44] Controlled surface poisoning studies[21] combined with DFT (Ref. 38) suggest that O_i injection occurs especially efficiently at sites of tri-coordinated Zn atoms that lie inside a triangular pit and occupy only a few percent of the total surface sites. The structure in aqueous environments is unknown, although OH is likely to adsorb stably due to the propensity of Zn to form bonds with OH.[45] Oxygen injects under liquid water as O; no hydrogen enters the material.[2] The polar Zn-term (0001) and O-term (000$\bar{1}$) orientations lead to injection rates roughly a factor of three greater than the nonpolar (10$\bar{1}$0) orientation.[2]

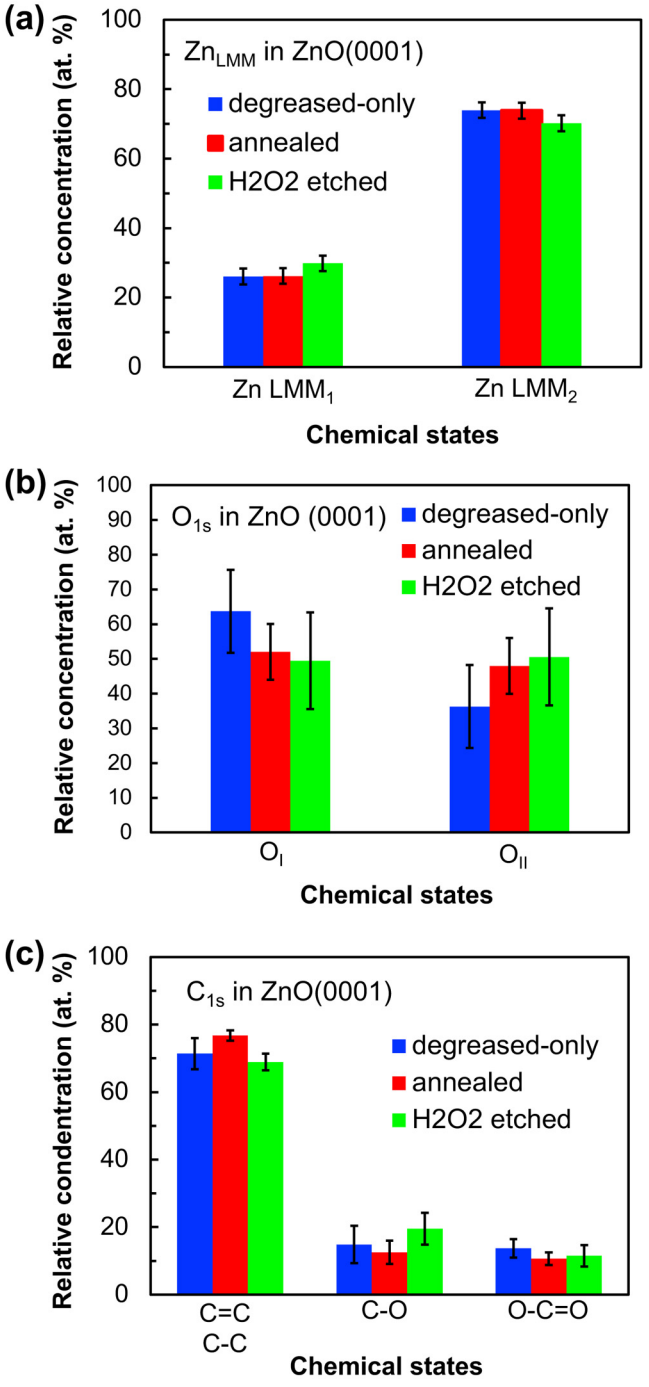

FIG. 9. Relative concentrations of different chemical states as measured by XPS on ZnO(0001) for (a) Zn, (b) O, and (c) C in response to various surface treatments. From left to right, bars signify degreased-only (blue), vacuum annealed (red), and wet etched (green). Confidence intervals were derived from data taken at various points on several specimens.

A. Interpretation of XPS and AFM measurements

For the surfaces examined here, carbon is the only foreign element that is ever present in significant amounts. Indeed, large amounts of adventitious carbon appear in the *ex situ* XPS spectra of all specimens examined. Such carbon undoubtedly resides on all the surfaces both before and after the diffusion experiments. For both TiO_2 and ZnO, the total amount of carbon remains largely invariant with treatment procedure, as do the chemical states of C, O, and Ti or Zn. Of course, we were unable to investigate *in situ* the amounts that were present while isotopic diffusion took place. Yet in the liquid water of *p*H 7, it seems unlikely that the total amount of adsorbed carbon would change appreciably upon the removal of the surface from immersion.

For TiO_2(110), AFM shows that the surfaces became slightly smoother when treated with aqueous NH_4OH or vacuum annealing compared to the degreased-only protocol. This smoothening correlates with increases in F and L. The number of AFM scans is small, but there is little physical reason to believe that these small decreases in roughness induce the sizable increases in F and L. Moreover, it seems doubtful that the roughness varies randomly for a fixed surface treatment in a way that explains the variations in all three parameters that motivate this work.

For ZnO(0001), vacuum annealing leaves the surface roughness largely unaffected compared to degreasing only, but wet etching with H_2O_2 increases the roughness by nearly an order of magnitude. Yet, both the H_2O_2 and vacuum annealing treatments give statistically significant larger values of F and L than degreasing only. In these experiments, the change roughness does not correlate with variations in profile parameters.

In short, the XPS and AFM measurements offer little evidence that either surface roughness or the generic presence of carbon on the surface causes the variability that is consistently observed in F and L across several oxides and crystallographic orientations. Thus, the variability probably originates from factors not readily detectable with the characterization tools employed here.

B. Possible mechanism for variability in *F*

The following paragraphs build an argument that, for TiO_2(110), ZnO(0001), and perhaps other oxide surfaces, a distribution of geometries and corresponding activation barriers characterize both the creation of injectable O and subsequent injection of O_i. Significant contributions to these distributions originate from especially active sites that correspond to steps, kinks, and sometimes sites characterizing specific surface reconstructions. These especially active sites represent only small fractions of the surface but are especially vulnerable to poisoning by adventitious adsorption. This poisoning is sensitive to minute details of the preparation procedure, whose effects propagate into outsized influences on the injection rate averaged over the surface.

As argued elsewhere,[2] the rate-limiting step for overall injection lies kinetically upstream from the creation of O_i from adsorbed O. Evidence comes from the effective activation energy for O_i injection, which is 0.2–0.3 eV as shown by Fig. 3 for TiO_2(110) and previous literature for both TiO_2(110) and ZnO(0001).[2] This range lies considerably below the barriers for the elementary step that

converts adsorbed O into O_i—roughly 0.8 eV for TiO_2 and 1.1 eV for ZnO.[2] The removal of H from adsorbed OH is more difficult than the removal of H from adsorbed H_2O[38,39] and offers a natural candidate for the rate-limiting step.

The energy barrier for H removal in liquid water is not known for either TiO_2 or ZnO, although the reaction occurs spontaneously for TiO_2 at highly alkaline *p*H levels (>13).[39] An extensive literature review of chemical reactivity on oxide surfaces suggests that a typical oxide surface presents a variety of defect sites—O surface vacancies, steps, kinks, and others—that have lower barriers for dissociation reactions than typical terrace sites. Although such sites typically occupy only a small fraction of the total surface area, they exert outsized and sometimes dominant effects on surface reactivity. Precisely because such sites exhibit enhanced reactivity, they may also be especially vulnerable to poisoning.

These especially active sites presumably obey the principle of Sabatier that optimal catalysis occurs when interactions with OH, O, and H are intermediate in strength—not so weak to inhibit dissociation, but not strong enough to induce poisoning. Identifying such sites requires a better understanding of reaction enhancement by site geometries and electronic properties, the influence of surface reconstruction and crystallographic misorientation, and the effects of the preparation method and adsorption of C in various forms. These questions mimic those typically asked for heterogeneous catalysis, and the techniques employed here can address them only obliquely.

Similar ideas apply to the elementary-step injection of interstitials in semiconductor surfaces, as well as the reverse process of interstitial annihilation. Annihilation requires no dissociation of a source molecule species such as OH or O_2 and, therefore, provides less ambiguous evidence for injection site poisoning. An example is N adsorbed on Si(100), which decreases the annihilation probability of Si interstitials by two orders of magnitude at only 1% of a monolayer.[3] Sulfur cuts the annihilation rate of titanium interstitials (Ti_i) in TiO_2(110) by a significant amount at only 10% of a monolayer.[46] The nature of the especially active sites remains unknown, but they clearly occupy only a small fraction of the surface. The injection rate of O_i from ZnO(0001) decreases by a factor of five with sulfur present at only 7% of a monolayer.[21] However, no definitive determination could be made whether such sites acted primarily to dissociate gaseous O_2 or to facilitate elementary-step injection.

For surfaces in contact with liquid water, sites that are especially active for injection may or may not be the same as those that are especially active for the dissociation of OH into H and injectable O. The principle of Sabatier presumably still applies to sites for elementary-step injection, but this time, the pertinent species are the injectable atom and the interstitial. Again, precisely because such sites exhibit enhanced capacity for injection, they may also be especially vulnerable to poisoning.

C. Possible mechanism for variability in λ and *L*

The following paragraphs build an argument that, for TiO_2(110), ZnO(0001), and perhaps other oxide surfaces, variability in *F* propagates into both λ and *L* because the latter parameters depend upon the concentrations of trapping sites for O_i that can become saturated.

O_i trapping mechanisms in both TiO_2 and ZnO are understood only partially, but it is clear that more than one species participates, likely in a specimen-dependent way. Single crystals of both materials typically contain V_O as the dominant O-related native defect.[47] In general, the concentrations of V_O can vary widely[48] depending upon synthesis history.[16] Other native point and extended defects exist in both materials, whose reactivity is unknown. Variable concentrations of extended defects from initial mechanical polishing by the manufacturer may also contribute trapping variability. Extrinsic hydrogen is a ubiquitous adventitious impurity in oxides.[49,50] DFT calculations show that O_i–H_i complexes are stable.[2] Depending on how much H exists in a given specimen, the details of O_i–H_i complexation will vary.

Many of these traps exist in limited concentrations and can react with O_i only once. If *F* is sufficiently large, such traps will become fully saturated—a process that will begin near the surface and progress over time deeper into the bulk. Saturated traps no longer impede the in-diffusion of O_i. Since λ depends upon trapping behavior throughout the profile, one may expect that λ increases as *F* increases. The functional form of the increase will depend upon the details of the trapping chemistry and the concentrations of various traps. Also, *F* itself almost certainly decreases over time as O_i concentrations increase near the surface, leading to increased rates of back-diffusion and annihilation at the surface. Nevertheless, a general correlation between *F* and λ should be expected. Likewise, saturation effects should lead to a correlation between *F* and *L*.

Figure 10 shows that both λ and *L* exhibit correlations with *F* for both TiO_2 and ZnO. Because the functional form of the correlation is not known *a priori*, the figure plots all quantities in logarithmic units. This approach enables linear fits for functional forms that are linear, power law, or exponential. The resulting graphs can, indeed, be fitted with lines.

Figure 10 shows that the variation in *L* with *F* differs from that for λ. *L* depends mainly upon trapping behavior at the leading edge of the profile. A smaller fraction of traps may be saturated in that region. Moreover, large differences in the effective diffusivity of $^{16}O_i$ and $^{18}O_i$ due to statistical effects[37] complicate the behavior. The isotopic disparity in diffusivity enables $^{16}O_i$ to race far ahead of $^{18}O_i$, which biases the isotopic composition of interstitials at the leading edge of the interstitial diffusion front toward ^{16}O. Hence, the dependence of *L* on *F* may be expected to differ from that for λ.

Indeed, Fig. 3 shows one manifestation of this difference. *F* remains constant for TiO_2 prepared by NH_4OH etching vs vacuum annealing. *L* also remains constant, but λ exhibits a statistically significant change. TiO_2 vacuum annealing in O_2 removes essentially all V_O,[37] resulting in the loss of that kind of trap. The concentrations of various extended defects also shift upon annealing,[46] and the concentration of H may be affected as well. Evidently, these alterations in trapping behavior manifest in λ but not *L*.

D. Wet etching: Possible mode of action

As suggested above, preparation procedures that optimally facilitate the overall process of O_i injection must generate a

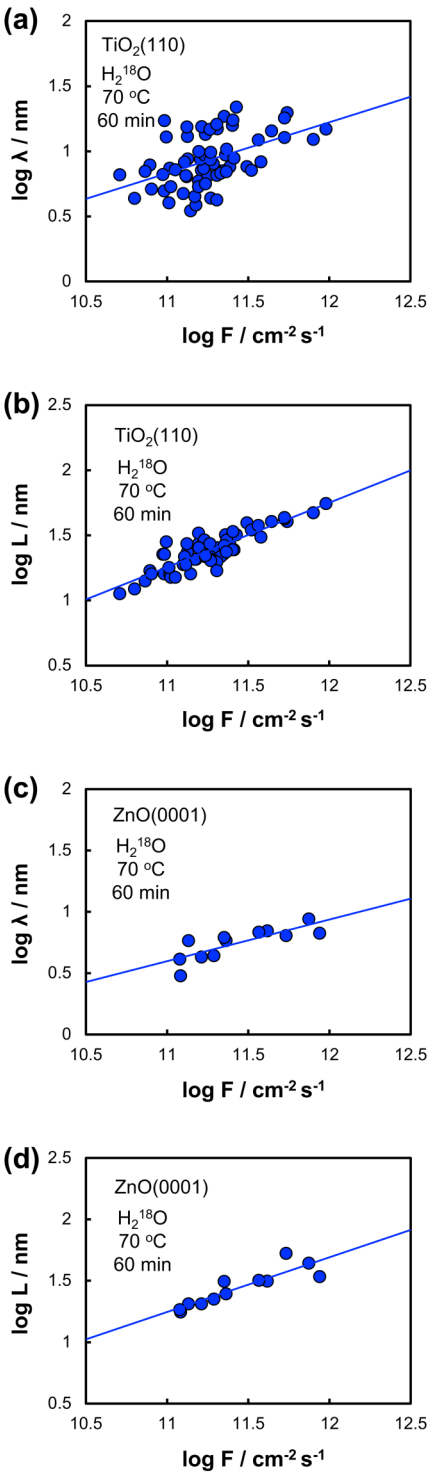

FIG. 10. Plots of log(λ) and log(L) vs log(F) for (a) and (b) TiO_2(110) and (c) and (d) ZnO(0001). The respective slopes are 0.39 ± 0.09 and 0.49 ± 0.03 for TiO_2 and 0.34 ± 0.08 and 0.44 ± 0.07 for ZnO.

constellation of sites that, in aggregate, optimize both the dissociation of OH into H and injectable O, and the subsequent injection of O as O_i. Surface poisons must be removed, and also the optimal constellation of sites must be generated. Since the distribution of sites optimizing the dissociation of OH may differ from that, which optimizes injection, it is plausible that the application of certain preparation procedures is best in terms of treatment time, temperature, or etchant concentration.

For example, this work has shown that such "best" values appear as a function of both time and concentration for H_2O_2 acting on ZnO(0001). Generally speaking, aqueous H_2O_2 serves as an oxidant through the formation of the hydroperoxide ion HO_2^- (Refs. 31 and 51) and is also acidic. ZnO is readily etched by H_2O_2 (Refs. 31 and 52) as well as by either acidic[53,54] or basic[55,56] solutions. Foreign adsorbates may become soluble by either the direct oxidation or dissolution of the substrate, and the latter typically shows a monotonic linear correlation with etching time.[31] The nonmonotonic behavior of the profile parameters in ZnO with increasing H_2O_2 concentration at 80 °C points to a complicated mechanism. The ineffectiveness of NH_4OH, which yields an alkaline solution capable of dissolving ZnO and also finds use with III–V semiconductors,[57,58] indicates clearly that substrate dissolution is only one factor in the effectiveness of H_2O_2. Higher etching temperatures (80 °C) improve the overall injection rate, yet the increased roughening promoted by such temperatures[31] is probably not a factor.

For TiO_2, mineral acids such as phosphoric (H_3PO_4),[25] sulfuric (H_2SO_4),[59] and hydrofluoric acid (HF)[60,61] readily etch the substrate but almost certainly leave behind unwanted foreign elements as poisons. NH_4OH and related bases such as NaOH and Na_3PO_4 all dissolve TiO_2,[62] with Na_3PO_4 being an order of magnitude more active than NaOH, which, in turn, is an order of magnitude more active than NH_4OH. Only NH_4OH was examined in the present work because of the possibility to desorb the ammonium cation as NH_3, thereby lowering the possibility of leaving behind poisons. This etchant has no special capacity for oxidation and presumably enabled the simple dissolution of the substrate and creation of the right constellation of sites. Notably, the efficacy was largely removed by the addition of H_2O_2, either together with the NH_4OH or in sequence after it.

V. SUMMARY AND CONCLUSIONS

The results presented here suggest that experimental variability in measuring O_i injection rates from TiO_2 and ZnO probably results from the adsorption of adventitious carbon that poisons small concentrations of nonterrace surface sites that are especially active for dissociating H_2O to injectable O or in converting injectable O into O_i. This poisonous adsorption of C acts directly on the net injection flux but also propagates indirectly into the penetration depth and mean diffusion length. The mechanism for that propagation probably involves the progressive saturation of O_i traps beginning near the surface, which occurs less extensively as the injected flux decreases. We surmise that, in the absence of special measures to exclude carbonaceous species during surface preparation and water immersion, the combination of poisoning and progressive trap saturation will lead to substantial experimental

variability in O_i injection and penetration across a wide variety of oxides. The details will depend upon the particular constellation of injection sites and bulk trapping species that exist within a given specimen.

ACKNOWLEDGMENTS

This work was supported by the U.S. National Science Foundation under Grant No. DMR 17-09327. SIMS, XPS, and AFM measurements were performed in the Materials Research Laboratory Central Research Facilities, University of Illinois at Urbana-Champaign.

AUTHOR DECLARATIONS

Conflict of Interest

The authors have no conflicts to disclose.

Author Contributions

Heonjae Jeong: Conceptualization (supporting); Formal analysis (equal); Investigation (equal); Methodology (equal); Writing – original draft (lead); Writing – review & editing (equal). **Edmund G. Seebauer:** Conceptualization (lead); Formal analysis (equal); Funding acquisition (lead); Investigation (equal); Methodology (equal); Project administration (lead); Supervision (lead); Writing – review & editing (equal).

DATA AVAILABILITY

The data that support the findings of this study are available from the corresponding author upon reasonable request.

REFERENCES

[1]H. Jeong and E. G. Seebauer, J. Phys. Chem. Lett. **13**, 9841 (2022).
[2]H. Jeong, E. Ertekin, and E. G. Seebauer, ACS Appl. Mater. Interfaces **14**, 34059 (2022).
[3]E. G. Seebauer, K. Dev, M. Y. L. Jung, R. Vaidyanathan, C. T. M. Kwok, J. W. Ager, E. E. Haller, and R. D. Braatz, Phys. Rev. Lett. **97**, 055503 (2006).
[4]E. Chason *et al.*, J. Appl. Phys. **81**, 6513 (1997).
[5]K. F. McCarty, J. A. Nobel, and N. C. Bartelt, Nature **412**, 622 (2001).
[6]I. E. Wachs and B. M. Weckhuysen, Appl. Catal. A **157**, 67 (1997).
[7]P. M. Fahey, P. B. Griffin, and J. D. Plummer, Rev. Mod. Phys. **61**, 289 (1989).
[8]M. E. Ingebrigtsen, A. Y. Kuznetsov, B. G. Svensson, G. Alfieri, A. Mihaila, U. Badstübner, A. Perron, L. Vines, and J. B. Varley, APL Mater. **7**, 022510 (2019).
[9]M. D. McCluskey, J. Appl. Phys. **127**, 101101 (2020).
[10]Z. Wang and L. Wang, EcoMat **3**, e12075 (2021).
[11]Y. Zhang *et al.*, Appl. Phys. Lett. **117**, 052406 (2020).
[12]H. J. Kang *et al.*, Nat. Mater. **6**, 224 (2007).
[13]J. Wang, R. Chen, L. Xiang, and S. Komarneni, Ceram. Int. **44**, 7357 (2018).
[14]D. Zu, H. Wang, S. Lin, G. Ou, H. Wei, S. Sun, and H. Wu, Nano Res. **12**, 2150 (2019).
[15]M. K. Nowotny, L. R. Sheppard, T. Bak, and J. Nowotny, J. Phys. Chem. C **112**, 5275 (2008).
[16]X. Wu, D. B. Migas, X. Li, M. Bosman, N. Raghavan, V. E. Borisenko, and K. L. Pey, Appl. Phys. Lett. **96**, 172901 (2010).
[17]D. Kim, K. Y. Lee, M. K. Gupta, S. Majumder, and S. W. Kim, Adv. Funct. Mater. **24**, 6949 (2014).
[18]X. Wang *et al.*, Phys. Rev. B **99**, 054106 (2019).
[19]W. Dong *et al.*, J. Mater. Chem. A **7**, 16728 (2019).
[20]P. Gorai, A. G. Hollister, K. Pangan-Okimoto, and E. G. Seebauer, Appl. Phys. Lett. **104**, 191602 (2014).
[21]M. Li and E. G. Seebauer, J. Phys. Chem. C **120**, 23675 (2016).
[22]P. Gorai, A. G. Hollister, and E. G. Seebauer, Appl. Phys. Lett. **103**, 141601 (2013).
[23]A. Janotti and C. G. Van de Walle, Phys. Rev. B **76**, 165202 (2007).
[24]H. Jeong and E. G. Seebauer, J. Phys. Chem. C **126**, 20800 (2022).
[25]S. Okazaki, T. Ohhashi, S. Nakao, Y. Hirose, T. Hitosugi, and T. Hasegawa, Jpn. J. Appl. Phys. **52**, 098002 (2013).
[26]A. G. Hollister, P. Gorai, and E. G. Seebauer, Appl. Phys. Lett. **102**, 231601 (2013).
[27]H. Jeong, M. Li, J. Kuang, E. Ertekin, and E. G. Seebauer, Phys. Chem. Chem. Phys. **23**, 16423 (2021).
[28]W. Vandervorst, Appl. Surf. Sci. **255**, 805 (2008).
[29]M. G. Dowsett, Appl. Surf. Sci. **203–204**, 5 (2003).
[30]A. Merkulov, P. Peres, S. Choi, F. Horreard, H.-U. Ehrke, N. Loibl, and M. Schuhmacher, J. Vac. Sci. Technol. B **28**, C1C48 (2010).
[31]Y. Wang, T. Wu, M. Chen, L. Su, Q. Zhang, L. Yuan, Y. Zhu, and Z. Tang, Appl. Surf. Sci. **292**, 34 (2014).
[32]F. Meng, F. Ge, Y. Chen, G. Xu, and F. Huang, Surf. Coat. Technol. **365**, 2 (2019).
[33]O. Dulub, L. A. Boatner, and U. Diebold, Surf. Sci. **519**, 201 (2002).
[34]C. Lennon, R. B. Tapia, R. Kodama, Y. Chang, S. Sivananthan, and M. Deshpande, J. Electron. Mater. **38**, 1568 (2009).
[35]W. Li, L. Fang, G. Qin, H. Ruan, H. Zhang, C. Kong, L. Ye, P. Zhang, and F. Wu, J. Appl. Phys. **117**, 145301 (2015).
[36]H. Jeong, E. G. Seebauer, and E. Ertekin, J. Chem. Phys. **153**, 124710 (2020).
[37]H. Jeong, E. Ertekin, and E. G. Seebauer, Langmuir **36**, 12632 (2020).
[38]R. L. Kurtz, R. Stock-Bauer, T. E. Msdey, E. Román, and J. De Segovia, Surf. Sci. **218**, 178 (1989).
[39]S. P. Bates, G. Kresse, and M. J. Gillan, Surf. Sci. **409**, 336 (1998).
[40]P. J. D. Lindan, N. M. Harrison, and M. J. Gillan, Phys. Rev. Lett. **80**, 762 (1998).
[41]E. V. Stefanovich and T. N. Truong, Chem. Phys. Lett. **299**, 623 (1999).
[42]P. M. Kowalski, B. Meyer, and D. Marx, Phys. Rev. B **79**, 115410 (2009).
[43]P. Gorai, E. G. Seebauer, and E. Ertekin, J. Chem. Phys. **144**, 184708 (2016).
[44]O. Dulub, U. Diebold, and G. Kresse, Phys. Rev. Lett. **90**, 016102 (2003).
[45]A. Wander and N. M. Harrison, J. Chem. Phys. **115**, 2312 (2001).
[46]K. L. Gilliard-AbdulAziz and E. G. Seebauer, Phys. Chem. Chem. Phys. **20**, 4587 (2018).
[47]F. M. Pinto, V. Y. Suzuki, R. C. Silva, and F. A. La Porta, Front. Mater. **6**, 260 (2019).
[48]F. Gunkel, D. V. Christensen, Y. Z. Chen, and N. Pryds, Appl. Phys. Lett. **116**, 120505 (2020).
[49]M. D. McCluskey, M. C. Tarun, and S. T. Teklemichael, J. Mater. Res. **27**, 2190 (2012).
[50]H. Li and J. Robertson, J. Appl. Phys. **115**, 203708 (2014).
[51]S. Sreekantan, L. C. Wei, and Z. Lockman, J. Electrochem. Soc. **158**, C397 (2011).
[52]A. Nakamura and J. Temmyo, J. Appl. Phys. **109**, 093517 (2011).
[53]K. Takahashi, H. Funakubo, N. Ohashi, and H. Haneda, Thin Solid Films **486**, 42 (2005).
[54]S. Pearton, W. Lim, F. Ren, and D. Norton, ECS Trans. **6**, 501 (2007).
[55]N. J. Nicholas, W. Ducker, and G. V. Franks, Langmuir **28**, 5633 (2012).
[56]X. Gan, X. Li, X. Gao, and W. Yu, J. Alloys Compd. **481**, 397 (2009).
[57]C. Bryce and D. Berk, Ind. Eng. Chem. Res. **35**, 4464 (1996).

[58]M. V. Lebedev, D. Ensling, R. Hunger, T. Mayer, and W. Jaegermann, Appl. Surf. Sci. **229**, 226 (2004).
[59]J. Ohkubo, Y. Hirose, E. Sakai, S. Nakao, T. Hitosugi, and T. Hasegawa, Jpn. J. Appl. Phys. **50**, 018002 (2011).
[60]R. Nakamura, N. Ohashi, A. Imanishi, T. Osawa, Y. Matsumoto, H. Koinuma, and Y. Nakato, J. Phys. Chem. B **109**, 1648 (2005).
[61]D. C. Hennessy, M. Pierce, K.-C. Chang, S. Takakusagi, H. You, and K. Uosaki, Electrochim. Acta **53**, 6173 (2008).
[62]S. E. Ziemniak, M. E. Jones, and K. E. S. Combs, J. Solution Chem. **22**, 601 (1993).
[63]See the supplementary material at https://www.scitation.org/doi/suppl/10.1116/6.0002467 for diffusion results for ZnO(0001) after several H_2O_2 etching procedures and XPS narrow-scan spectra for TiO_2(110) and ZnO.